# Lab on a Chip 2018

**PAPER** 

DOI: 10.1039/C7LC01344B

# Impedance-based real-time position sensor for lab-on-a-chip devices.

B. Brazey, <sup>a</sup> J. Cottet, <sup>b,c</sup> A. Bolopion, <sup>a</sup> H. Van Lintel, <sup>b</sup> P. Renaud <sup>b</sup> and M. Gauthier <sup>a</sup>

This paper presents the theoretical and experimental development of an integrated position sensor for Lab-On-a-Chip devices. The interest for single cell analysis is growing. However, this requires to monitor and control cell displacements in real-time during their journey in the chip. Due to the high number of cells that must be monitored at the same time, classical vision-based sensors are not suitable. This paper aims to present an alternative based on impedance measurement. The position of the cells is obtained from the variation of impedance measured between two electrodes. This technique presents several advantages: the sensor is integrated into the chip, the measurement electrodes are compatible with the fabrication process of actuation electrodes for dielectrophoresis, the sampling time of the sensor is high and the position of the cells can be obtained in real time. This article highlights the concept of position-sensitive impedance sensing. The design of the chip, and in particular of the electrodes, is discussed to improve the sensitivity and repeatability of the measurement. The issue of real-time detection in a noisy environment is solved by using an Extended Kalman Filter. As a first proof of concept this article presents experimental validation on a 1D case to determine the longitudinal position of 8.7 µm diameter beads in a channel.

#### 1 Introduction

Among the various areas of cell analysis, there is an increasing attractiveness for single cell analysis  $^1$ . The complex nature of tissues has motivated the development of tools for single-cell genomic, transcriptomic and multiplex proteomic analyses  $^2$ . In addition, many applications are foreseen in the study of the immune system  $^3$ .

To go beyond classical fluorescence-activated cell sorting, and in particular to offer a wide range of cell analysis tools (based for example on its mechanical, electrical and fluorescence properties), a number of Lab-On-a-Chip (LOC) devices have been developed. They have undergone a strong development in recent years for cell study and sorting <sup>4–6</sup>. The low production cost and the small sample volumes enhance their attractiveness for both cell sorting and characterization.

Most of these devices exploit dielectrophoresis (DEP) <sup>7</sup>, microfluidics <sup>8–10</sup> and/or electrical impedance measurement <sup>11</sup> to separate or characterize the cells. Dielectrophoresis-based methods are carried out when the electrical properties of the cells can be used as a discriminant criterion. Microfluidics are most often used when the cells can be differentiated by their size or their density. Impedance measurement has a large place in cell characterization. Electrical impedance spectroscopy (EIS) is commonly exploited to characterize the electrical properties, the size or the morphology of the cells <sup>12,13</sup>. A model in EIS describing a cell electrical behavior has been given <sup>14,15</sup>. At low frequencies, the

cell membrane, which is equivalent to a capacitance, prevents the electric field lines from penetrating the cell. When the signal frequency increases, the total impedance decreases since the membrane capacitance tends to be short-circuited. Internal properties such as the electrical resistance of the cytoplasm can then be evaluated. These analyses are mostly performed either to get statistical data on a large cell population, or to get precise measurement of a single cell. However, single cell analysis requires to perform measurement on each single cell of a large cell population, to combine knowledge about the individual properties of the cells with statistical analysis.

One of the main challenges of single cell analysis is to analyze a large number of cells in a restricted time. As an example, to analyze around 200 000 cells in around 35 minutes, 100 cells per second must be tested. It necessitates to be able to perform high speed trajectory control so that a large number of cells can be tested per second, and to parallelize the analysis. A conceptual view of such cell sorters is depicted in Figure 1. The cell flow is split through different distribution levels to perform cell analysis in parallel in tens of bioreactors.

Actuation of the chip can be performed in parallel using dielectrophoretic actuation. However sensors must be used to measure the trajectory of the particle in real-time. Most of the works use vision feedback <sup>16–18</sup>. However, classical vision-based sensors have limited field of view <sup>19</sup>. Indeed, with a high magnification, (e.g. 20x) the field of view is reduced (typically 0.5 x 0.5 mm²) compared to the size of the optical objective (e.g 25 mm diameter). Because of the huge ratio between the vision range and the objective size only a few parts of the chip surface (typically 0.04 %) are visible simultaneously with the camera. As single cell analysis only makes sense if we are able to massively parallelize the analysis or the treatment, the density of test zones on a chip has to be maximized. By using cameras, the density of test zones on the

<sup>&</sup>lt;sup>a</sup>FEMTO-ST Institute, AS2M department, Univ. de Bourgogne Franche-Comté CNRS, 24 rue Savary, F-25000 Besançon, France. E-mail: benoit.brazey@femto-st.fr

 $<sup>^</sup>b$ Microsystems Laboratory, Ecole Polytechnique Federale de Lausanne, EPFL, BM 3.124 Station 17, Lausanne, Switzerland.

 $<sup>^{</sup>c}$ Univ Lyon, Ecole Centrale de Lyon, CNRS, AMPERE, F-69130, Ecully, France

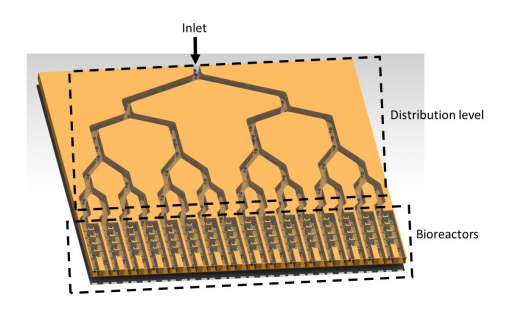


Fig. 1 Conceptual view of a cell sorter for single cell analysis. The total cell population is split to perform analysis in parallel in several tens of bioreactors.

chip is highly limited by the optical objective size (as the test zone has to be concentrated in the 0.04 % visible part of the chip).

In this paper, we propose to develop a proof of concept of an original alternative to vision consisting in impedance measurement. Impedance measurements are made on electrodes which can be easily integrated on Lab-On-a-Chip devices to perform parallelized sensing. In EIS, a lack of precision regarding the position of the cell between the electrodes may induce errors in the cell characterization, particularly when dynamic characterization is performed <sup>20</sup>. Consequently, the dependence of the measured impedance on the cell position between the measurement electrodes is desired to be as low as possible in cell characterization devices. In this paper, we propose to exploit this position dependence to get a position sensor. Currently, impedance measurements are also used to localize particles <sup>21–25</sup> or to estimate their velocity <sup>26</sup>. These current works consist in detecting the presence of a particle closed to two electrodes by detecting an impedance peak. The principle is also extended to two pairs of electrodes in order to determine locally the particle velocity. The current methods are limited to a single measure of the position or of the velocity from which a trajectory can be extrapolated based on a model of the flow. In the hypothesis of a high speed manipulation of cells, the cells are actuated by coupling fluidic and dielectrophoretic forces, which magnitude can potentially vary abruptly in time and space. In this sense, a punctual and fixed in space measurement cannot be invoked for continuous trajectory error correction due to a poor estimation (model errors or disturbances) of the flow or the dielectrophoretic force. In this paper, we propose a method to measure the whole particle trajectory based on a compromise between a model of the flow and the real-time impedance measurement.

Several issues have to be confronted regarding this approach. First, the electrodes must be designed to ensure the sensitivity of the sensor with respect to the position of the cell between the electrodes. Numerical simulations are performed to propose an electrode design dedicated to position sensing. Second, contrarily to most impedance-based applications, signal processing must be performed on-line and consequently should not introduce delays. Extended Kalman Filters (EKF) are well suited to real-time localization 27,28, and have already been applied to impedance measurements to extract information from a noisy signal <sup>29–31</sup>. In this paper, an Extended Kalman Filter is implemented to extract the position based on noisy impedance measurements. first proof of concept, the proposed approach is validated experimentally on 8.7 µm diameter polystyrene beads in a 1D case to determine their longitudinal position in real-time in a channel.

This paper is organized as follows: Section 2 is dedicated to the methodology of impedance measurement for position detection and to sensor design. Section 3 deals with signal processing. An Extended Kalman Filter is implemented and experimental validation of the proposed approach is performed using calibrated microbeads in Section 4. Section 5 discusses the obtained results, in particular as regards real-time detection of cell position. Section 6 concludes this paper.

# Impedance measurement for sensitive and repeatable position detection

#### 2.1 Electrical impedance measurements

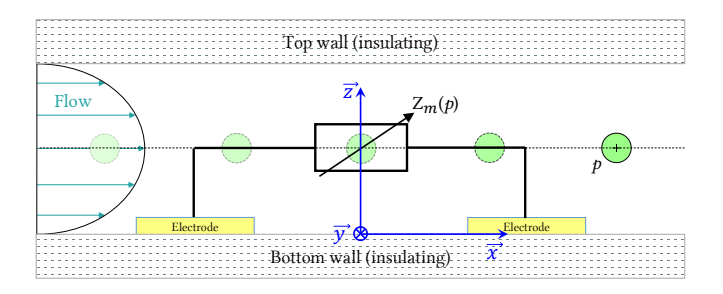


Fig. 2 Simplified equivalent circuit model, illustrating the dependency of impedance on cell position. The impedance of the system (composed of the medium and the cell) is modeled as a variable impedance, the value of which depends on the cell position in the channel.

Electrical impedance measurement consists in applying a lowamplitude voltage U as the excitation signal between electrodes and measuring the resulting current intensity I. The impedance Zof the system is then deduced:

$$Z = \frac{U}{I} \tag{1}$$

When a fluidically actuated cell is moving between the electrodes, the impedance varies due to the difference of the electrical properties between the cell and the medium. The measured impedance of the system composed of the fluid and the particle can be represented as a variable impedance  $Z_m$ , as illustrated in Figure 2.

The value of the variation depends on the impedance of the medium  $Z_0$  which will be referred to as the baseline and a variable impedance due to the presence of the cell  $Z_c(p)$  where prepresents the position of the cell along the longitudinal axis x of the channel with respect to the electrodes:

$$\left\{ \begin{array}{ll} Z_m(p=\infty)=Z_0 & \text{no cell between the electrodes} & \text{(2)} \\ \\ Z_m(p)=Z_0+Z_c(p) & \text{cell detected} \end{array} \right.$$

In this paper we propose to exploit the variation of impedance for position sensing in LOCs. As a first proof of concept, this

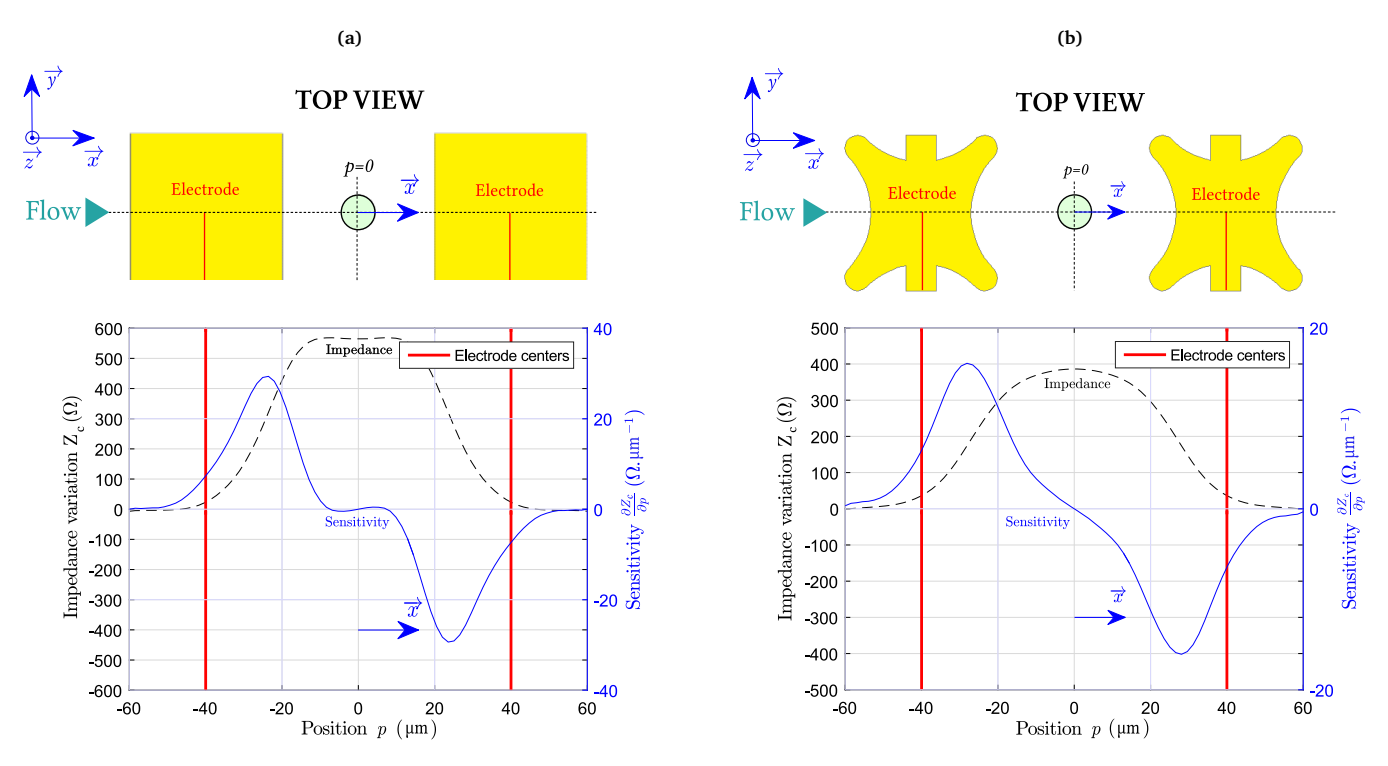


**Fig.** 3 FEM simulations of the variation of impedance due to the presence of an insulating bead between two electrodes as a function of its longitudinal position in a fluidic channel. Two electrode designs are considered: a) a classical electrode design (square-shaped) and b) a star-shaped design. The parameters of the simulation are: medium: PBS ( $\sigma_s = 1.6 \text{ S/m}$ ,  $\varepsilon_s = 80$ ), channel width: 40 μm, channel height: 20 μm, object: 8 μm diameter bead ( $\sigma_b = 10^{-14} \text{ S/m}$ ,  $\varepsilon_b = 4$ , spacing between the electrodes: 80 μm, altitude of the bead: 10 μm (center of the channel height).

article focuses on the position of a particle along the longitudinal axis x of the channel. As will be explained in the next sections the lateral position of the cell as well as its height will be controlled using focusing electrodes, as is commonly done in DEP actuated LOC  $^{13}$ .

As mentioned in the introduction, at low frequencies, the cell membrane, which is equivalent to a capacitance, prevents the electric field lines from penetrating the cell. Under these conditions, the electrical behaviour of a cell is similar to that of an insulating microbead of identical size. Consequently, studying cell position detection or microbead position detection is equivalent. The rest of the paper will focus on bead simulations and measurements.

#### 2.2 Sensitivity of position detection

Sensitivity is the ratio between the measured signal (output) and the measured property (input). In classical EIS, since the measured properties are cell characteristics, the variation of impedance with respect to the position of the cell should be as low as possible, as it is well known in the literature  $^{26}$ . In this work, sensitivity definition (impedance variation per unit of length along the x axis) requires a variation of impedance with respect to the position of the cell. In order to maximize the detection range of the sensor, the sensitivity should be different from zero.

Finite Element Method (FEM) simulations are performed with Comsol software. A classical example involving an insulating 8 µm diameter bead passing through a microchannel in a PBS (phosphate buffered saline) solution is studied. The results obtained for two representative designs of electrodes, squareshaped and star-shaped (with smooth tips), are presented in Figure 3. The square shaped electrodes are the ones commonly used in EIS (Figure 3.a). However, this design is not suitable for position sensing due to the 20 µm zone in which the impedance is almost constant. On the contrary, sensitivity using star-shaped electrodes (Figure 3.b) is non-zero except at the exact center between the electrodes. It means that impedance directly depends on the position of the bead. Providing an adequate response, this geometry is retained for the impedance-based position sensor proposed in this paper. Finding the optimal electrode layout design is out of the scope of this article. However, several designs have been tested to select the star-shaped electrode layout. They are presented and compared in the Appendix, Section 7.

#### 2.3 Repeatability of electrical impedance measurement

As mentioned previously, this article focuses on a first proof of concept which consists in detecting the position of a bead along one direction, the longitudinal axis x of the channel. In this section, the goal is to identify the influence of the position of the bead along the other axes on impedance measurement, and to ensure the repeatability of the experiment. FEM simulations have been conducted to analyse the impedance variation due to the height of the cell in the channel. Results are presented in Figure 4. For beads close to the bottom wall of the channel ( $z = 4.1 \mu m$ ),

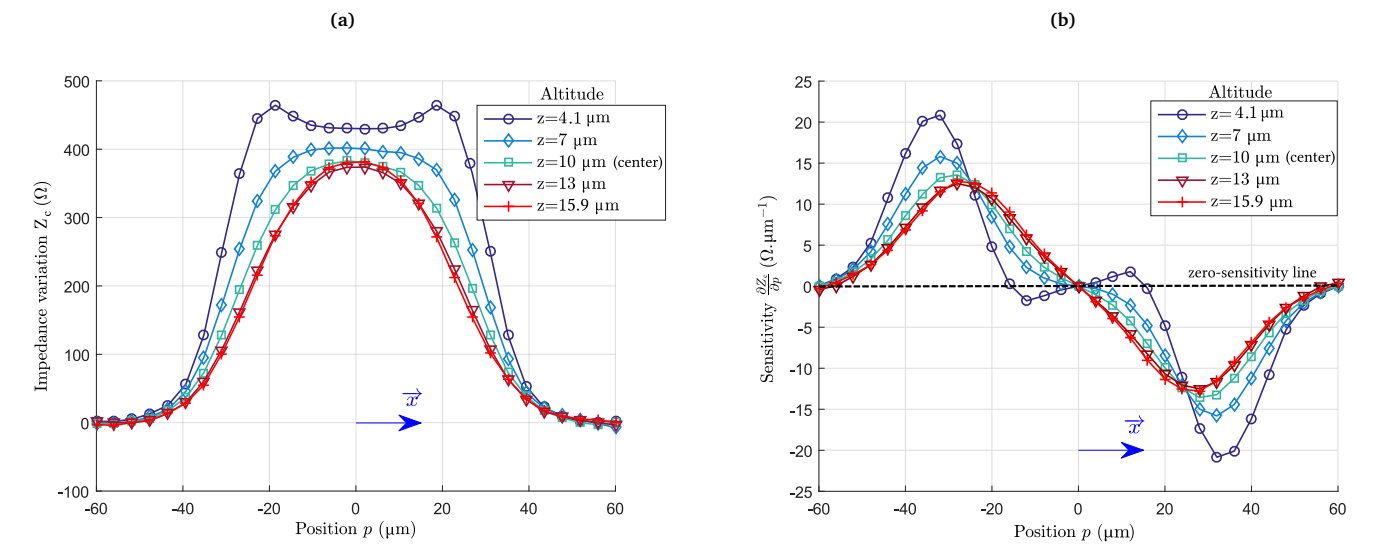
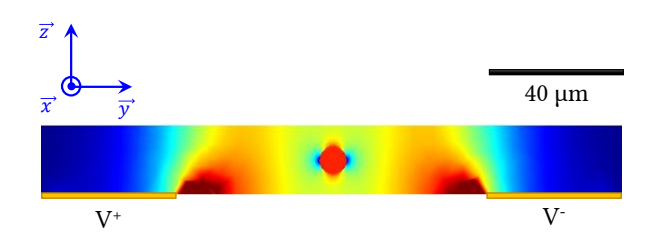


Fig. 4 Simulation of (a) the variation of impedance and (b) sensitivity of the sensor induced by the passage of a 8 μm diameter cell in PBS for the star-shaped electrode geometry at different altitudes in a 20 μm high channel.



**Fig. 5** Electric field intensity in the microchannel when an insulating bead is present while DEP focusing electrodes are activated. The dielectrophoretic force displaces the bead to the low electric field regions. The bead finds its equilibrium position at the center of the channel section.

the plot of dependence of impedance on position exhibits three inflection points (corresponding to a sensitivity equal to zero), which makes the position detection more complicated. tain repeatable impedance measurements, the height of the beads should be controlled and they should be elevated, by at least a few micrometers, to ensure a good sensitivity and the shape of the impedance variation. Similarly, FEM simulations (not presented in this document) show that the impedance also depends on the lateral position of the beads in the channel. Consequently, the beads will be centered in the channel section to obtain repeatable results. To do so, liquid electrodes 13 are used to focus the beads along the y axis (which means that the beads are at the center of the channel width) and to control the height of the particle. Liquid electrodes are coplanar electrodes fabricated on the bottom of dead-end chambers placed on the side of the main channel. The insulating walls and ceiling of the channel guide the electric field lines in the liquid into the main channel, and determine the electric field distribution inside the microstructure. A phase opposition potential on the electrodes generate a negative dielectrophoretic force which acts on the beads, and focuses them toward the low electric field regions. Figure 5 presents the electric field intensity for a microbead located between the liquid electrodes. The dielectrophoretic force maintains the beads at the center of the channel width (y axis) due to the generated field gradient. Furthermore, the bead presence interferes with the homogeneous vertical (z axis) electric field generated by the liquid electrodes. The induced electric field gradient is source of a vertical dielectrophoresis force which controls the z position of the beads. In the rest of the paper, beads crossing the detection zone are then assumed centered along the channel width (y axis) and their height is controlled so that they are in the middle of the channel (along the z axis).

# 3 Real-time detection

The goal of this section is to detect in real-time the presence of a bead between the electrodes. The challenge is to isolate the signal of interest (ie the variation of impedance  $Z_c$ ) from a noisy and drifted signal (the measured impedance  $Z_m$ ).

#### 3.1 Experimental setup

The experimental setup is composed of a microfluidic chip (Figure 6), with actuation and sensing units.

The microfabricated chip is composed of a layer of electrodes and a microfluidic channel. A lift-off process involving Cr/Au layers (15 nm / 120 nm) on a 500  $\mu m$  thick glass wafer is performed to design the electrodes. A 20  $\mu m$  thick SU8 layer is deposited by spin coating and patterned by photolithography to make the channel. The chip is mechanically sealed by pressing a PDMS (polydimethylsiloxane) cover layer on the SU8 microchannel, and is mounted on a printed circuit board to connect the electrodes to the sensing and actuation units.

The actuation unit's purpose is to translate the beads inside the channel and make them cross the detection area centered in the channel section. A pumping station (pressure controller *Elveflow OB1* and syringes) induces a laminar flow of approximately  $800 \ \mu m/s$  that guides the beads across the chip channel.

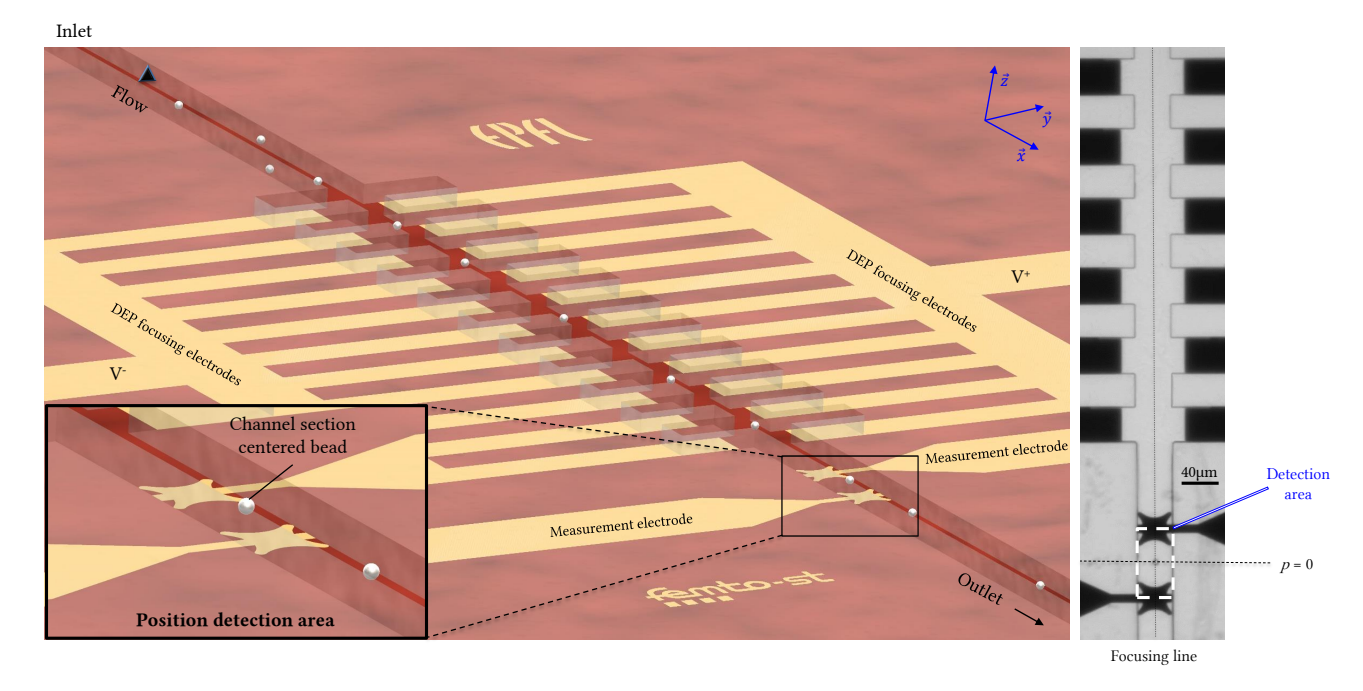


**Fig. 6** Illustration (left side) and photograph (right side) of the chip. The fluidic actuation guides the beads into the channel, and DEP focusing electrodes center them in the channel section. The position of the beads is detected by impedance measurement (in the detection area).

A low frequency generator associated to amplifier and inverter mountings applies phase opposition potentials on the DEP focusing electrodes that maintain the beads at the center of the channel section. The potentials applied on the electrodes are sine waves of respectively  $V^+=23~{\rm V_{pp}}$  and  $V^-=-23~{\rm V_{pp}}$ , with a frequency of 70 kHz.

The sensing unit aims at detecting the position of the beads. The measurement electrodes are powered with an AC signal of 1.6  $V_{pp}$  at a frequency of 500 kHz. A pre-amplifier followed by a lockin amplifier (*Zurich Instruments HF2TA* and *HF2LI*) are used to measure the impedance between the measurement electrodes. This measurement unit filters the signal. In our particular experiments, we assume that the bead travel time between the center of each detection electrodes is around 100 ms. The sampling rate is set to  $10\times10^3$  samples per second and the low pass filter time constant of the impedance spectroscope is set to 70  $\mu s$ .

To calibrate the impedance based position sensor a camera is used. A vision platform (*Leica* inverted microscope and *Allied Vision* camera, model *Stingray*) records images. *VISP* (Visual Servoing Platform) libraries are used for image processing, to detect the position of the beads. This calibration is performed off-line. To increase the variation of the measured impedance  $Z_m$  when the bead is located between the measurement electrodes, the bead and the medium must have significantly different electrical properties. A conductive solution (diluted PBS,  $\sigma_s = 1 \text{ S/m}$ ,  $\varepsilon_s = 80$ ) and infinite impedance beads (*Estapor*, 8.7 µm diameter calibrated polystyrene beads considered as perfectly insulating) are chosen.

#### 3.2 Signal extraction

The chip is filled with the solution of diluted PBS in which beads are injected. The bead concentration in the medium is approximately 10<sup>6</sup> beads per milliliter. They are moved inside the chip by the flow. The impedance between the detection electrodes is measured, and the result is presented in Figure 7.a. Two phenomena can be noticed in this figure: (i) there is a drift in the measured signal and (ii) high magnitude peaks, corresponding to the presence of beads or impurities between the measurement electrodes, are present.

The drift is mainly due to a change of conductivity which is, among other causes, due to the change of temperature. Heat changes the conductivity of the medium which changes the value of the baseline  $Z_0$ . One solution to evaluate this baseline despite the noise and the drift is to apply a moving median to the signal. This method is similar to a low-pass filtering and it is robust to rare events, which here are the variation of impedance induced by the bead passages. Furthermore, the moving median can be stopped while a peak is detected to minimize estimation error on the baseline value. Integration period of the moving median has to be low compared to the drift constant time and high compared to bead passage and noise constant time. A 100 ms moving median is applied on the measured signal  $Z_m$ . The drift is compensated by subtracting this average value from the current measured value  $Z_m$ . Result of this drift compensation is displayed in Figure 7.b. It can be noticed that this filtering only necessitates to get information on the previously measured values and it is thus compatible with real-time signal processing. As an alternative this drift issue can be addressed by performing a differential measurement <sup>12</sup>. This method consists in subtracting the impedance measured by an additional electrode, identical

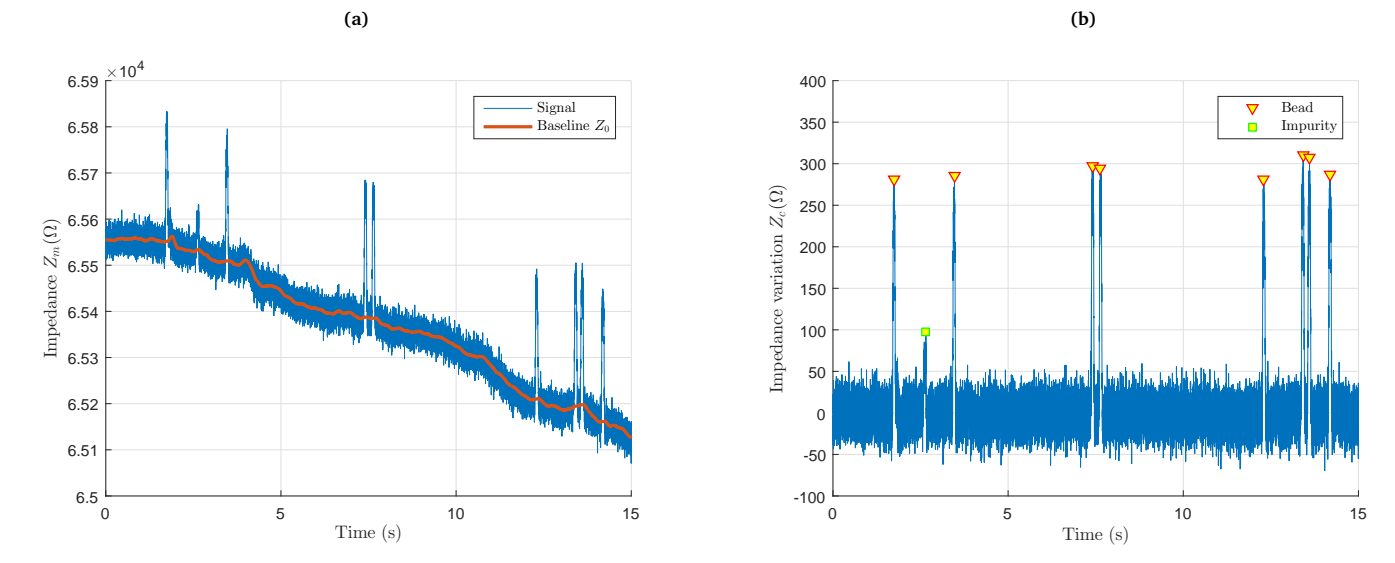


Fig. 7 Real-time extraction of the signal of interest. (a) The measured signal  $Z_m$  is filtered and thresholded to obtain the baseline  $Z_0$  by applying a moving median. (b) The two signals are substracted to obtain the variation of impedance  $Z_c$  due to the passage of the beads.

and not influenced by the presence of the particle, from the signal of interest  $Z_m$ .

From this signal with compensated drift (Figure 7.b) it is now necessary to detect the variation of impedance  $Z_c$  due to the presence of a bead. To do so, a threshold is set on the measured impedance  $Z_m$  above which a bead is considered as present. The baseline evaluation using the moving median is then stopped until the bead leaves the detection zone (i.e.  $Z_m$  decreases below the given threshold). The impedance variation  $Z_c$  due to the presence of a bead is extracted by subtracting the estimated value of the baseline  $Z_0$  at the instant the bead is detected from the signal  $Z_m$ . The detected beads are indicated in Figure 7.b by the triangle markers. A small deviation on the peak amplitudes for two different beads can be noticed. It can be due to an error between the real and measured baseline, to a variation in the altitude of the beads in the channel, or to impurities. In particular the small amplitude peak at around 2.6 s is due to the passage of an impurity, as confirmed by the video recording.

# Real-time position estimation

#### Principle of the Extended Kalman Filter

The previous section aimed at performing signal processing to compensate for the drift, and to detect the passage of beads. The goal is now to get information about the position of the bead based on the impedance measurement when a bead is detected. Two main challenges must be overcome: (i) the signal noise (ii) the fact that there is no unique relation between the impedance value and the position of the bead since the impedance variation is symmetrical with respect to the point located at the center between the two measurement electrodes. This is especially an issue when the bead is located near the center between the two measurement electrodes since despite the design chosen for the electrodes the variation of impedance remains low (see Figure 3.b).

The classical method, which consists in calibrating the sensor off-line and then in using a look-up table which gives, for a measured impedance value, the corresponding position, cannot be applied in this paper. Indeed, the signal is noisy and the relation between the measured impedance and the position of the bead is not one-to-one. As depicted in Figure 8, a given value of impedance corresponds to two positions of the bead. It is not possible, from the sole measurement, to determine which one is the correct one. This is why a state observer based on the Extended Kalman Filter Kalman filtering consists of two (EKF) equations is proposed. recursive steps aiming to provide an estimation of a state  $x_k$ . The first one is a prediction step in which an estimate of the state is provided, considering only knowledge about the dynamics of the system studied. When a new (noisy) measurement is available, the estimated state is corrected. This is the second step. For each iteration k the state vector  $x_k$  and the measurement vector  $y_k$  are:

$$\begin{cases}
 x_k = \begin{bmatrix} p_k \\ v_k \end{bmatrix} \\
 y_k = \begin{bmatrix} Z_c(p_k) \end{bmatrix}
\end{cases}$$
(4)

where  $p_k$  is the bead position,  $v_k$  its velocity and  $Z_c(p_k)$  the impedance variation induced by the bead as defined in the previous sections.

The system is described by the state and observation models. The state model (6) corresponds to the mathematical model of the system, while the observation model (7) corresponds to the measured data:

$$\begin{cases} x_k = f(x_{k-1}, u_{k-1}) + w_{k-1} \\ y_k = h(x_k) + v_k \end{cases}$$
 (6)

where v is the measurement noise and w represents the disturbances which affect the system (also called process noise).

The Extended Kalman Filter is an extension of the Kalman filter dedicated to nonlinear systems. At each time step, the non-linear functions describing the mathematical model and the observation model of the system (f and h in Eq. 6 and 7) are linearized. These linearized functions are processed using the standard Kalman filter equations. Details about the theory of observers and Extended Kalman Filter can be found in the litterature  $^{32,33}$ .

The state model input vector  $u_k$  is related to the fluidic actuation. f represents the bead dynamics. It can be estimated based on the knowledge of the physical equations ruling the system and in particular on Newton's second law and fluid velocity. h is the observation model. It will be identified during the calibration phase.

These elements (state and observation models, measurement noise and disturbance characteristics) of the filter are determined in the next sections.

#### 4.1.1 State model f

The first equation of the state model, which is the mathematical model, is obtained by considering that the derivative of position is velocity. The second equation is obtained by assuming that the velocity of the bead is equal to the one of the fluid. This means that at each instant the bead is in equilibrium (the sum of the forces applied on it is null). The DEP force applied by the measurement electrodes is considered negligible. The state model is thus linear and defined as follows:

$$\begin{bmatrix} \hat{p}_k \\ \hat{v}_k \end{bmatrix} = \begin{bmatrix} 1 & \Delta t \\ 0 & 0 \end{bmatrix} \begin{bmatrix} \hat{p}_{k-1} \\ \hat{v}_{k-1} \end{bmatrix} + \begin{bmatrix} 0 \\ v_f \end{bmatrix}, \tag{8}$$

where  $v_f$  is the fluid velocity,  $\Delta t$  the time interval between two measurements and  $u_k = \begin{bmatrix} 0 & v_f \end{bmatrix}^T$  is the state model input vector. A rough estimation of  $v_f$  will be set at the initialization of the detection. This value is then updated at each time step based on the velocity of the bead estimated by the Extended Kalman Filter. The Kalman Filter will correct this estimation based on new impedance measurement.

#### 4.1.2 Observation model h

To identify the observation model, which corresponds to the measured, filtered and interpolated data, the proposed sensor is calibrated. The calibration consists in finding the dependence of the measured impedance on the position of the bead. The impedance spectrometer *Zurich Instruments* provides impedance measurement as a function of time. The position of the bead as a function of time is estimated by an additional external position sensor (in this case: a camera). This camera is needed only for the calibration phase, which is performed just once, off-line. The sampling period of the camera being lower than the spectroscope's one, the positions obtained from the camera are interpolated such that the period between two impedance measurements and two position measurements with the camera is equal.

Positions as a function of time provided by the camera and impedance measurements as a function of time provided by the impedance spectroscope are then correlated to obtain the

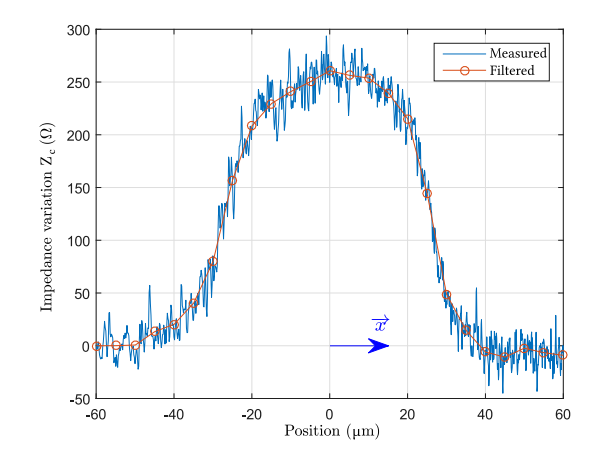


**Fig. 8** The impedance variation as function of the bead position  $Z_c = h(p)$  is experimentally obtained by camera and impedance spectrometer data correlation. The curve is smoothed to remove the noise and recorded as the observation model.

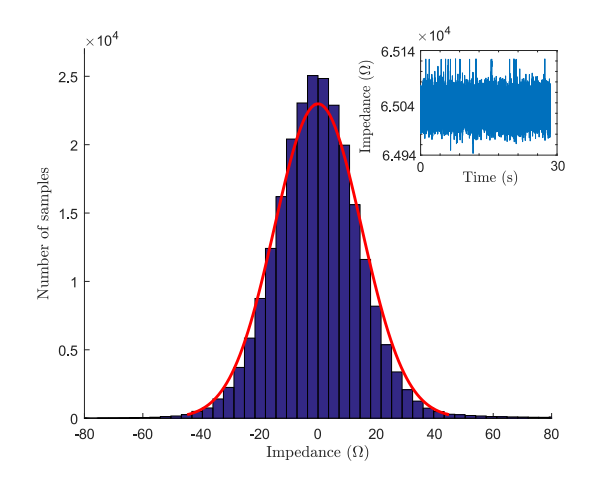


**Fig. 9** Measurement noise distribution (the mean value has been subtracted to the signal). The signal is recorded for a sufficient duration (30 s) to obtain a statistical distribution of the noise.

impedance as a function of the position, as presented in Figure 8. The experimentally obtained impedance variation is smoothed using a zero-phase low-pass filter. These data are used to define the h function of the observation model.

# 4.1.3 Covariance of the measurement noise v

The reliability of the observation model depends on the measurement noise ( $\nu$ ). It varies as a function of the averaging time of the lock-in amplifier, which determines the bandwidth of the impedance measurement. This noise is characterized experimentally.

The covariance matrix R of the measurement noise is necessary for the implementation of the Extended Kalman Filter. R depends on the standard deviation of the measurement noise  $S_v$ :

$$R = \left[ S_{\nu}^{2} \right] \tag{9}$$

To identify  $S_{\nu}$  experimentally, the impedance of the medium is measured over 30 s without bead nor actuation. The mean value of the noise is computed, and it is subtracted from the signal (see

inset of Figure 9). From this measurement noise the standard deviation is evaluated as presented in Figure 9. It follows a gaussian distribution with a standard deviation of  $S_{\nu}=14.5~\Omega$ . This reinforces the choice of the Extended Kalman Filter since Kalman filtering provides an optimised observation when noise is gaussian.

#### **4.1.4** Covariance of the disturbances *w*

Similarly, trust in the state model is related to the covariance matrix Q of the disturbance (w). Disturbances related to the position and the velocity of the bead are assumed not to be correlated  $^{34,35}$ .

This leads to:

$$Q = \begin{bmatrix} S_{w_1}^2 & 0\\ 0 & S_{w_2}^2 \end{bmatrix},\tag{10}$$

where  $S_{w_1}$  and  $S_{w_2}$  are the covariances of the disturbances related to the state model (8). The first relation of the state model corresponds to the fact that the derivative of position is velocity. We assume that no disturbance affects this relation. Thus  $S_{w_1}$  is set to 0:

$$Q = \begin{bmatrix} 0 & 0 \\ 0 & S_{w_2}^2 \end{bmatrix}, \tag{11}$$

 $S_{w_2}$  represents the standard deviation of the disturbance linking the fluidic force applied to the bead and its velocity. It can hardly be identified analytically, so this parameter is tuned empirically. One of the main issues while using Extended Kalman Filtering is to find a tradeoff between the trust in the mathematical model (given by the state model) and the trust in the measured data (given by the observation model). If too much trust is given to the mathematical model the system cannot correct errors due to inappropriate modeling or to inherent disturbance in the system that modifies the trajectory of the bead. On the contrary, measurements are subjected to noise and are a source of errors in the low sensitivity region at the center of the electrodes (see Figure 3.b and Section 5). Consequently, we choose here to give equal trust in both the mathematical model and measured data. This tuning is performed by selecting the appropriate disturbance covariance Q. The higher the covariance, the lower is the trust that the filter gives to the mathematical model. The value  $S_{w_2}$  is chosen experimentally. It is set to  $80 \mu m/s$  as it provides a precise estimation of the position of the bead.

# 4.2 Implementation of the bead tracking

Figure 10 presents the different steps of signal processing and position estimation. The total impedance  $Z_m$  is measured and signal processing is performed to compensate for the drift, as explained in Section 3.2. When a bead is detected, the variation of impedance due to the presence of the bead  $Z_c$  is sent to the Extended Kalman Filter. Based on both this measurement and the state model, the state vector is computed.

For each new bead j detected, an initial state vector  $\hat{x}_0^j$  must be defined. Concerning the initial position of the bead, it is assumed that  $p_0^j = -40~\mu \text{m}$ . It corresponds to the position of the center of the first measurement electrode. As depicted in Figure 3, this

is the first position at which the bead is detected. The initial velocity  $\hat{v}_0^j$  is more complex to determine. Two cases must be considered: the initial velocity of the first bead  $\hat{v}_0^0$  and the initial velocity of the bead j,  $\hat{v}_0^j$ , where  $j \neq 0$ .

The velocity of the first bead  $\hat{v}_0^0$  is set to an arbitrary value (here 1200 μm/s) chosen according to the settings of the pressure controller. Controlling the flow velocity with a syringe pump would make it more straightforward to estimate the velocity of the particles, and thus the Kalman filter convergence would be faster since the initial state would be known more precisely. However, pressure controllers present several advantages, such as fast response time and high stability and pulseless flow. If the flow rate has to be known, it is still possible to integrate a flow meter with a feedback loop. The goal here is to show that the Kalman filter would converge despite a large error on the initial prediction of the particles velocity. This is why we did not consider controlling the flow rate precisely. In addition, the initial bead velocity estimation is voluntarily biased in this article (around 30% of error) to test the robustness of the method proposed in this paper. Thus the initial state vector  $\hat{x}_0^0$  is set to:

$$\hat{x}_0^0 = \begin{bmatrix} \hat{p}_0^0 \\ \hat{v}_0^0 \end{bmatrix} = \begin{bmatrix} -40 \ \mu\text{m} \\ 1200 \ \mu\text{m/s} \end{bmatrix}$$
 (12)

The initial velocity of the  $j^{th}$  bead is set to be equal to the velocity of the  $j-1^{th}$  bead. As the velocity of the bead is equal to the velocity of the flow this assumption holds if the variation of the flow velocity is low between the two beads. This is commonly true since the beads are separated by only a few seconds. To avoid noise the last estimated velocities of the  $j-1^{th}$  bead during its passage between the electrodes are averaged over 100 ms. Consequently, the  $j^{th}$  bead initial state vector is:

$$\hat{x}_0^j = \begin{bmatrix} \hat{p}_0^j \\ \hat{v}_0^j \end{bmatrix} = \begin{bmatrix} -40 \ \mu\text{m} \\ SMA(\hat{v}^{j-1}) \ \text{m/s} \end{bmatrix}$$
 (13)

where SMA is the simple moving average function, here applied on the previous bead estimated velocities.

Based on these initial state vectors  $\hat{x}_0^j$  (where j can be equal to 0), the filter provides at each iteration an estimation  $\hat{x}_k^j$  of the state vector exploiting the state and observation models, and their associated trust defined by the matrices Q and R. To improve the estimation of the position of the  $j^{th}$  bead (where j can be equal to 0), the state model is constantly updated. As previously presented, it is assumed that the bead velocity is equal to the velocity of the flow. Thus, at each time step, i.e. even during the bead passage, the velocity of the fluid  $v_f$  in Eq. (8) is updated based on the value of the bead velocity estimated by the Kalman Filter (see the feedback loop in Figure 10). To eliminate the influence of noise the velocity of the fluid  $v_f$  is assumed to be equal to the last 1000 estimated velocities of the bead. This corresponds to a moving average of  $\tau = 100$  ms. It consists, at time t, in averaging the estimated velocity between  $t - \tau$  and t to update the model. This method increases the convergence time of the filter, but stabilizes the estimation regarding punctual observation model errors. The

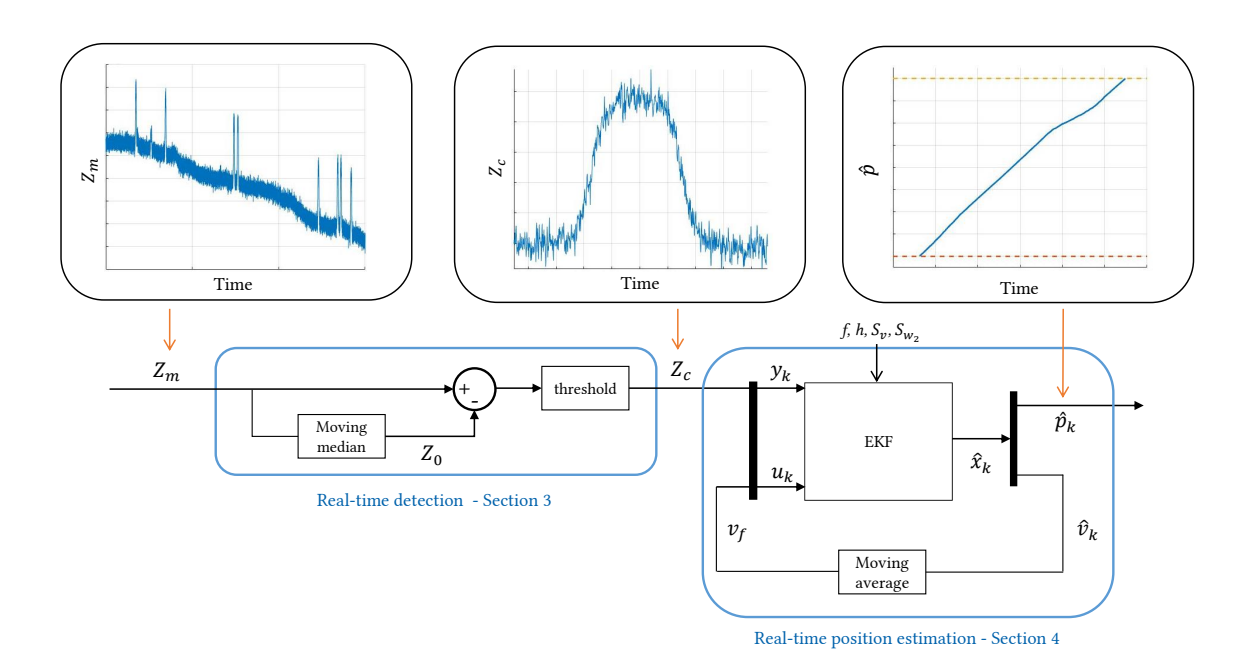


Fig. 10 Diagram presenting the principle of signal processing for position estimation based on impedance measurements. The first step consists in extracting the signal of interest, as explained in Section 3. Extended Kalman Filter is then implemented to estimate the state of the bead based on both the impedance measurement and knowledge about the state model. In particular it necessitates to know the velocity of the flow, which is considered equal to the velocity of the bead. This value is thus updated at each time step using the estimation provided by the Kalman Filter.

state model given by Eq. (8) is thus modified as:

$$\begin{bmatrix} \hat{p}_k \\ \hat{v}_k \end{bmatrix} = \begin{bmatrix} 1 & \Delta t \\ 0 & 0 \end{bmatrix} \begin{bmatrix} \hat{p}_{k-1} \\ \hat{v}_{k-1} \end{bmatrix} + \begin{bmatrix} 0 \\ SMA(\hat{v}) \end{bmatrix}. \tag{14}$$

# 4.3 Experimental position estimation of a bead

This section aims to discuss the position estimation obtained from impedance measurements as presented in the previous sections. It is compared to positions obtained from images given by a camera. The camera is here only used as a comparison and not for the impedance based position detection, apart from the calibration step that can be performed off-line (see Section 4.1.2).

Results are given in Figure 11. Figure 11.a presents the velocity of the beads flowing in the channel. Both the velocities obtained from impedance measurements and from images obtained by the camera are compared. Concerning the velocity obtained from impedance measurements, it is obtained by averaging the estimated bead velocities obtained by the Kalman Filter (100 ms integration time). As described in the previous section, averaging the estimated bead velocities allows to obtain a stable and continuously corrected value of fluid actuation for the state model. Velocity estimation starts at 1200 μm/s as defined in the input state vector  $x_0^0$  (Eq. 12). Then the feedback corrects this value. Despite the large initial error on the velocity, the filter estimation converges to the value obtained from the camera. As expected, the moving average induces a non negligible convergence time of the measurements obtained from impedance but it avoids the large variations due to noise. This convergence time can be set by tuning the moving average in Figure 10.

Figure 11.b (resp. Figure 11.c) presents the position estimation

of the first (resp. fifth) bead obtained both by impedance and by the camera. For the estimation based on impedance measurement the bead detection starts at  $p=-40~\mu m$ , which corresponds to the center of the first electrode and ends at  $p=40~\mu m$  which corresponds to the center of the second electrode. For a given bead, the position estimation initially tends to present large differences with vision detection. This might be due to several issues such as a lag in the bead detection since the impedance has to reach a given threshold so that the bead is detected. In addition, the magnitude of the difference with vision detection depends on the accuracy of the state model. Here, the difference with vision detection for the first bead position estimation is about  $10~\mu m$ , whereas this value is around 4  $\mu m$  and less after a few beads.

Vision detection does not rely on a state model, so there is no convergence time. However, vision presents several drawbacks, in addition to the size of the objectives that has been discussed earlier: with high magnification, the camera sampling rate (30 fps maximum) must be decreased to get a long enough exposure time due to the low amount of light reaching the camera. In our experiment, the sampling rate of the camera was set at about 15 fps. Since the bead passage lasts approximately 100 ms, the camera can provide only one image of the bead in the detection area. The plots of Figure 11, which depicts the position of the bead with respect to time are thus obtained using a linear interpolation between two available measurements. Currently, it is thus not possible to get in real time the position of the bead between the electrodes due to this low sampling rate. This approximation is consistent insofar as the fluid velocity undergoes very slow variations (considered as negligible over a period of 100 ms). The use of the impedance-based technique improves the

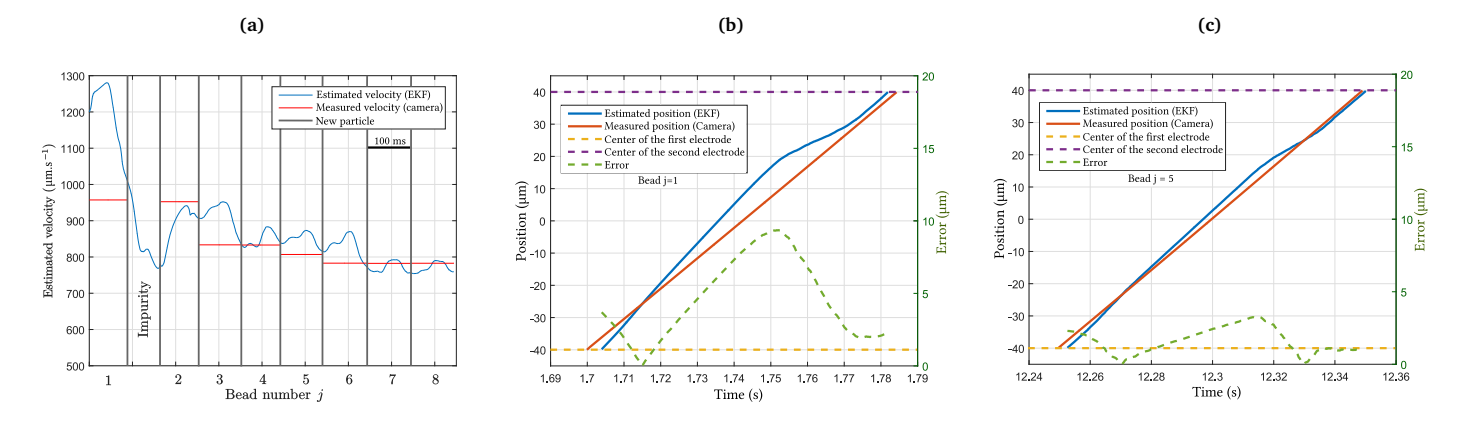


Fig. 11 Real-time position and velocity estimation using both impedance and vision feedback and associated differences. (a) The velocity of the first beads is highly overestimated using the proposed approach based on impedance measurements compared to vision due to the initial velocity value set to the Kalman filter ( $v_0^0$ ). It results in a difference of around 10 micrometers in the position estimation for bead j = 1 (b). As the Kalman filter corrects the value of velocity the estimation converges towards the velocity values obtained from the camera (a). The position estimation difference between impedance and vision based techniques remains below 4 micrometers for bead j = 5(c).

sampling rate of the position measurement: an impedancemeter such as the HF2LI from  $Zurich\ Instruments$  allows to get 210 x  $10^6$  samples per second, which is significantly higher than the commonly obtained camera rate of 30 images per second.

These results demonstrate that the impedance based approach is an attractive alternative solution to vision to provide integrated real-time position sensing inside LOCs.

### 5 Discussion

This paper presents the proof-of-concept of an impedance based position sensor to get the position of cells in Lab-On-a-Chip devices along one direction. To validate experimentally the concept, insulating microbeads with a calibrated diameter are used. However, impedance measurement is widely used on cells, and for the frequency of the excitation signal (500 kHz), their electrical behavior (high impedance) is similar to that of polystyrene beads due to their low conductivity. The position sensor should thus provide similar results on cells, under the hypothesis of a small dispersion in the radius of the cells, or that this radius has been determined beforehand, using measurements by impedance spectroscopy for example. In order to make the observation model insensitive to temperature, all measurement values are divided by the updated baseline magnitude. For the sake of clarity, this does not explicitly appear in the preceding conceptual description.

For this proof of concept, impedance measurements are post-processed. However, special care has been taken to develop tools compatible with on-line processing. The only step that is commonly realized off-line is the calibration step. Otherwise, all the signal processing steps are based only on previous measurements. In addition computation time is negligible (about 40  $\mu s$  per iteration). The proposed methodology can thus be readily transferred to perform on-line position estimation.

As discussed in Section 4.1.4, the relation between the measured impedance and the position of the bead is not one-to-one. It is thus not possible to use the classical method for position sensing, which consists in calibrating the sensor off-line and then using a look-up table to deduce the position from the measure-

ment only. Figure 12 illustrates this issue. Data previously used for position estimation (see Figure 11), are used again with a different filter tuning. Now the filter is tuned so that the trust in the state model is zero  $(S_{w_2} \to \infty)$ . This is equivalent to using only impedance measurements. It can be seen that the difference between the position obtained from impedance measurement and from the camera is huge when the bead is in the middle of the electrodes, where the sensitivity of impedance measurement is null. The position estimation can even estimate that the bead went backward (see Figure 12.b). This non unique relation between the measured impedance and the position of the bead justifies the use of a Kalman filter, which combines both knowledge of the state model and of impedance measurements. This work is thus the first step toward a fully integrated sensor for cell position detection in real-time in Lab-on-Chip devices.

We propose in this paper an original design of electrodes to obtain a position sensitive signal in the entire zone between the electrodes. An alternative consists in using the classical design (square-shaped electrodes) and reducing the spacing between the electrodes. The sensor response for such a configuration is described in the litterature <sup>26</sup>. This technique increases the mean sensivity of the sensor, but decreases the detection range.

# 6 Conclusions and perspectives

This paper presents a sensor dedicated to position estimation of cells in Lab-on-chip devices. It is based on measurements of the impedance between two electrodes. When a cell is present between these electrodes the impedance varies depending on the position of the cell with respect to the electrodes. A specific design of electrodes enables to enlarge the sensitivity distribution compared to classical designs. In order to estimate the cell position despite drift and signal noise, signal processing is proposed to detect the cell passage. A dedicated Extended Kalman Filter is implemented to estimate the position of the cell from the impedance measurements. It exploits both the measurement and knowledge about the behaviour of the cells.

This sensor has been experimentally tested on polystyrene

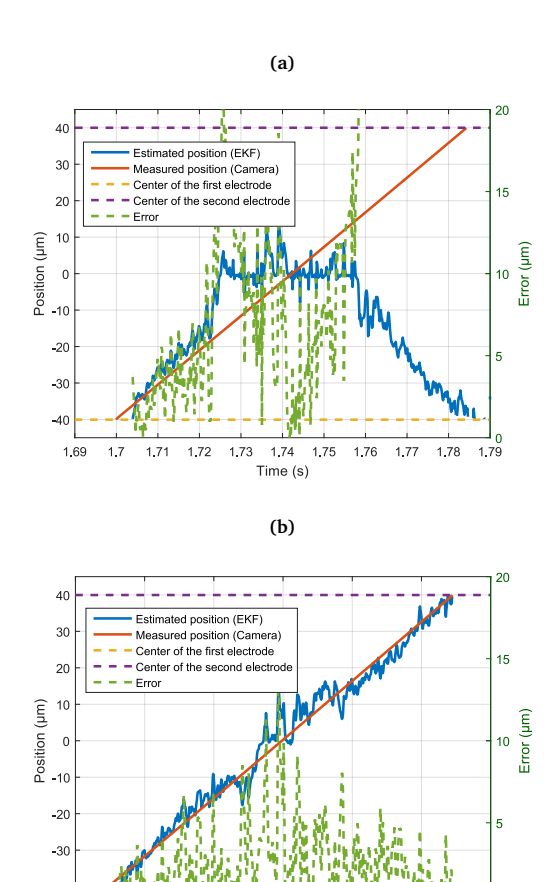


**Fig. 12** Real-time position and velocity estimation using both impedance and vision feedback and associated differences when no trust is given to the state model as a function of time for (a) bead j = 1 and (b) bead j = 5.

Time (s)

12.24

beads by means of post processed impedance measurements. It demonstrates the ability of the sensor to estimate the position of an object between two measurement electrodes along one direction. As discussed, this sensor can be easily applied to on-line cell position estimation since cells and insulating beads present similar electrical characteristics and the signal processing methods are compatible with real-time processing.

This paper is thus the first step towards the development of an innovative and integrated sensor for cell 3D position estimation based on impedance measurement. This proof of concept also opens the way for implementing 2D or 3D integrated position control in LOCs by exploiting the electrodes for both actuation (DEP) and sensing (impedance measurement).

# 7 Appendix - influence of the shape of the electrodes on the impedance measurement

Geometry		Sensitivity around the center	Number of zero- sensitivity points	Mean sensitivity $(\Omega/\mu m)$
	G1 (Classical)	No	1	14.0
X	G2 (Selected)	Yes	1	12.5
	G3	No	1	14.1
X	G4	Not significant	1	13.3
	G5	Yes	3	14.4
	G6	Yes	1	11.6

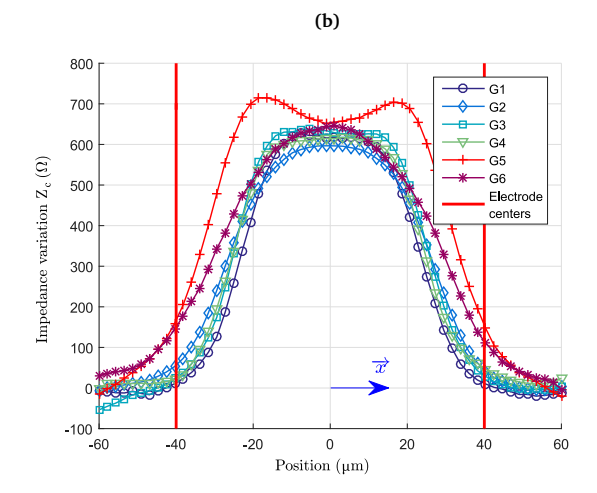
**Table 1** Comparison of the performances of different geometries of electrodes for position detection based on impedance measurements.

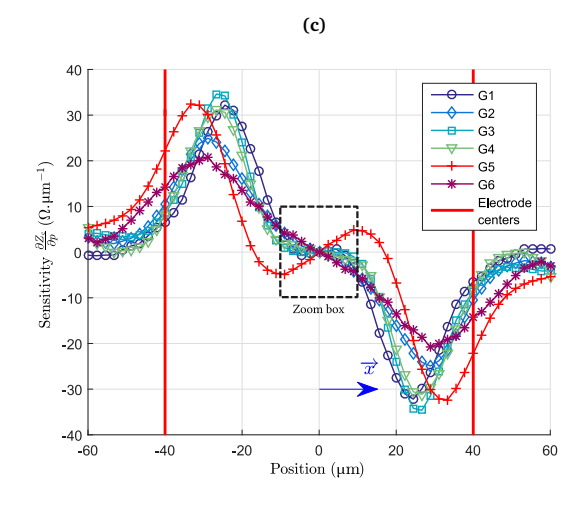
This section compares the impedance measurement obtained when a bead is flowing in the channel for different electrode designs. Several geometries of electrodes are tested, with different properties: concave or convex, with rounded or tapered shapes. Six geometries are compared in Table 1. Only the case for which the two electrodes are identical is considered. Two criteria are considered in the choice of a geometry: (i) the number of zerosensitivity points and (ii) the sensitivity of the signal around the center of the electrodes. Due to the symmetry of the detection area, which is composed of two identical electrodes, at least one zero-sensitivity point is expected in the center, between the two electrodes. Ideally, it should be the only zero-sensitivity point since errors in the reconstruction of the position are more likely to occur around these points. As an additional criterion to select the geometry of the electrodes, the mean sensitivity should be maximized.

Figure 13b presents FEM simulations of the impedance measured between the electrodes when a bead is flowing inside the channel. The parameters used for the simulation are the ones given in Section 2. One design, G5, presents 3 zero-sensitivity points (see Figure 13c). It is thus discarded. The designs G1, G3 and G4 present no (or not significant) sensitivity around the center of the sensor detection area (Figure 13d). They are discarded. Two designs, G2 and G6, are compatible with the above mentioned criteria. Since G2 has the highest mean sensitivity (Table 1), this geometry is selected as the measurement electrode design.

This comparison aims at finding a suitable design for position detection based on impedance measurement. This might not be







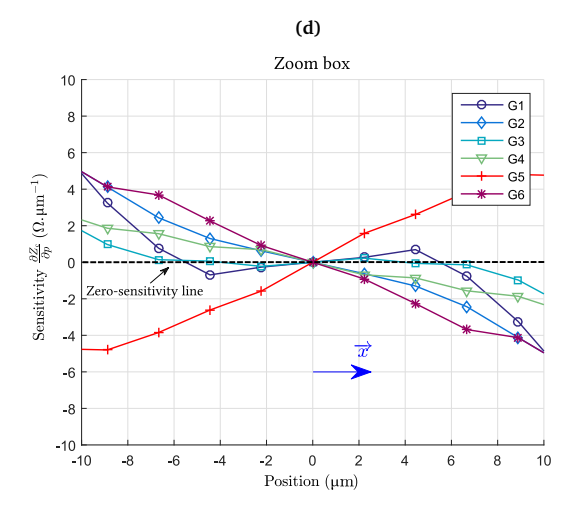


**Fig. 13** Simulation of the response of the sensor for different electrode designs. (a) Tested designs summary. (b) Variation of impedance as a function of the position of the bead. (c) Sensitivity of the sensor. (d) Zoom around the center of the detection area. Simulation parameters are identical to Section 2.

the optimal design, but full optimization is out of the scope of this article. It would necessitate advanced computation techniques such as the implementation of a genetic algorithm. Nevertheless, it can be noticed that concave shapes are likely to be satisfying designs.

## Acknowledgments

This work has been supported by:

- Labex ACTION project (contract "ANR-11-LABX-0001-01")
- French RENATECH network and its FEMTO-ST technological facility.
- Collegium SMYLE (SMart SYstems for a better LifE)
- Région Franche-Comté
- European ERDF Bourgogne-Franche-Comté Project "Projet FEDER MIMEDI"

#### References

- 1 "DEPArray<sup>TM</sup> Technology," http://www.siliconbiosystems.com, accessed: 2017-11-15.
- 2 J. R. Heath, A. Ribas, and P. S. Mischel, "Single-cell analysis tools for drug discovery and development," *Nat Rev Drug Discov*, vol. 15, pp. 204–216, 2016.
- 3 P. K. Chattopadhyay, T. M. Gierahn, M. Roederer, and J. C. Love, "Single-cell technologies for monitoring immune systems," *Nature immunology*, vol. 15, no. 2, pp. 128–135, 2014.
- 4 S. Lindstrom and H. Andersson-Svahn, "Overview of single-cell analyses: microdevices and applications," *Lab Chip*, vol. 10, pp. 3363–3372, 2010.
- 5 V. Lecault, A. K. White, A. Singhal, and C. L. Hansen, "Microfluidic single cell analysis: from promise to practice," *Current Opinion in Chemical Biology*, vol. 16, no. 3, pp. 381–390, Aug. 2012.
- 6 P. Ertl, D. Sticker, V. Charwat, C. Kasper, and G. Lepperdinger, "Lab-on-a-chip technologies for stem cell analysis," *Trends in biotechnology*, vol. 32, no. 5, pp. 245–253, 2014.
- 7 N. Lewpiriyawong and C. Yang, "Dielectrophoresis field-flow fractionation for continuous-flow separation of particles and cells in microfluidic devices," in *Advances in Transport Phenomena* 2011. Springer, 2014, pp. 29–62.
- 8 P. Sajeesh and A. K. Sen, "Particle separation and sorting in microfluidic devices: a review," *Microfluidics and Nanofluidics*, vol. 17, no. 1, pp. 1–52, 2014.
- 9 E. L. Jackson and H. Lu, "Advances in microfluidic cell separation and manipulation," *Current Opinion in Chemical Engineering*, vol. 2, no. 4, pp. 398 404, 2013.
- 10 A. Reece, B. Xia, Z. Jiang, B. Noren, R. McBride, and J. Oakey, "Microfluidic techniques for high throughput single cell analysis," *Current Opinion in Biotechnology*, vol. 40, pp. 90 – 96, 2016.
- 11 Y. Xu, X. Xie, Y. Duan, L. Wang, Z. Cheng, and J. Cheng, "A review of impedance measurements of whole cells," *Biosensors and Bioelectronics*, vol. 77, pp. 824 836, 2016.

- 12 S. Gawad, L. Schild, and P. Renaud, "Micromachined impedance spectroscopy flow cytometer for cell analysis and particle sizing," *Lab on a Chip*, vol. 1, no. 1, pp. 76–82, 2001.
- 13 M. Shaker, L. Colella, F. Caselli, P. Bisegna, and P. Renaud, "An impedance-based flow microcytometer for single cell morphology discrimination," *Lab Chip*, vol. 14, pp. 2548–2555, 2014.
- 14 S. Gawad, K. Cheung, U. Seger, A. Bertsch, and P. Renaud, "Dielectric spectroscopy in a micromachined flow cytometer: theoretical and practical considerations," *Lab on a Chip*, vol. 4, no. 3, pp. 241–251, 2004.
- 15 K. Cheung, S. Gawad, and P. Renaud, "Impedance spectroscopy flow cytometry: on-chip label-free cell differentiation," *Wiley Online Library, Cytometry Part A*, vol. 65, no. 2, pp. 124–132, 2005.
- 16 C. Jiang and J. K. Mills, "Planar cell orientation control system using a rotating electric field," *IEEE, Transactions on Mechatronics*, vol. 20, no. 5, pp. 2350–2358, 2015.
- 17 P. Benhal and J. Chase, "System identification and stochastic estimation of dielectric properties of a spherical particle using ac-induced electro-rotation," in *IEEE*, 20th International Conference on Process Control (PC), 2015, pp. 332–337.
- 18 J. Zemánek, T. Michálek, and Z. Hurák, "Feedback control for noise-aided parallel micromanipulation of several particles using dielectrophoresis," Wiley Online Library, Electrophoresis, vol. 36, no. 13, pp. 1451–1458, 2015.
- 19 M. Kharboutly and M. Gauthier, "High speed closed loop control of a dielectrophoresis-based system," in *IEEE, International Conference on Robotics and Automation (ICRA)*, 2013, pp. 1446–1451.
- 20 J. Claudel, M. Nadi, O. Elmazria, and D. Kourtiche, "Microfluidic biosensor for single cell high speed flow impedance spectroscopy," in *Proceedings of the 8th International Conference on Sensing Technology*, 2014, pp. 343–347.
- 21 G. Medoro, N. Manaresi, A. Leonardi, L. Altomare, M. Tartagni, and R. Guerrieri, "A lab-on-a-chip for cell detection and manipulation," *IEEE Sensors Journal*, vol. 3, no. 3, pp. 317–325, 2003.
- 22 J. Wu, Y. Ben, and H.-C. Chang, "Particle detection by electrical impedance spectroscopy with asymmetric-polarization AC electroosmotic trapping," *Microfluidics and Nanofluidics*, vol. 1, no. 2, pp. 161–167, May 2005.
- 23 P. Sabounchi, A. M. Morales, P. Ponce, L. P. Lee, B. A. Simmons, and R. V. Davalos, "Sample concentration and impedance detection on a microfluidic polymer chip," *Biomedical Microdevices*, vol. 10, no. 5, p. 661, May 2008.
- 24 M. Varshney and Y. Li, "Interdigitated array microelectrodes based impedance biosensors for detection of bacterial cells," *Biosensors and Bioelectronics*, vol. 24, no. 10, pp. 2951 – 2960, 2009.
- 25 C. Bernabini, D. Holmes, and H. Morgan, "Micro-impedance cytometry for detection and analysis of micron-sized particles and bacteria," *Lab Chip*, vol. 11, pp. 407–412, 2011.
- 26 V. Errico, A. D. Ninno, F. R. Bertani, L. Businaro, P. Bisegna,

- and F. Caselli, "Mitigating positional dependence in coplanar electrode Coulter-type microfluidic devices," *Sensors and Actuators B: Chemical*, vol. 247, pp. 580 586, 2017.
- 27 P. Bonnifait, P. Bouron, P. Crubillé, and D. Meizel, "Data fusion of four ABS sensors and GPS for an enhanced localization of car-like vehicles," in *IEEE, International Conference on Robotics and Automation.*, vol. 2, 2001, pp. 1597–1602.
- 28 S. Rezaei and R. Sengupta, "Kalman filter-based integration of DGPS and vehicle sensors for localization," *IEEE, Transactions* on Control Systems Technology, vol. 15, no. 6, pp. 1080–1088, Nov 2007.
- 29 K. Kim, S. Kang, M. Kim, S. Kim, Y. Lee, and M. Vauhkonen, "Dynamic electrical impedance tomography with known internal structures," *Inverse Problems in Engineering*, vol. 11, no. 1, pp. 1–19, 2003.
- 30 K. Kim, B. Kim, M. Kim, Y. Lee, and M. Vauhkonen, "Image reconstruction in time-varying electrical impedance tomography based on the Extended Kalman Filter," *IOP Publishing, Measurement science and technology*, vol. 12, no. 8, p. 1032, 2001.
- 31 M. Soleimani, M. Vauhkonen, W. Yang, A. Peyton, B. S. Kim, and X. Ma, "Dynamic imaging in electrical capacitance to-mography and electromagnetic induction tomography using a Kalman filter," *IOP Publishing, Measurement Science and Technology*, vol. 18, no. 11, p. 3287, 2007.
- 32 G. Besançon, *Nonlinear observers and applications*. Springer, 2007, vol. 363.
- 33 G. A. Terejanu, "Extended Kalman filter tutorial," *University at Buffalo*, 2008.
- 34 M. Vauhkonen, P. A. Karjalainen, and J. P. Kaipio, "A Kalman filter approach to track fast impedance changes in electrical impedance tomography," *IEEE Transactions on Biomedical En*gineering, vol. 45, no. 4, pp. 486–493, 1998.
- 35 I. Hassanzadeh and M. A. Fallah, "Design of augmented extended Kalman filter for real time simulation of mobile robots using Simulink," in *6th International Symposium on Mechatronics and its Applications*, 2009, pp. 1–6.